

# One-pot pyrolysis route to Fe–N-Doped carbon nanosheets with outstanding electrochemical performance as cathode materials for microbial fuel cell

Yong Sun<sup>1\*</sup>, Zezhen Zhang<sup>1,2</sup>, Yongming Sun<sup>2\*</sup>, Gaixiu Yang<sup>2</sup>

(1. College of Engineering, Northeast Agricultural University, Harbin 150030, China;

2. Guangzhou Institute of Energy Conversion, Chinese Academy of Sciences, CAS Key Laboratory of Renewable Energy, Guangdong Provincial Key Laboratory of New and Renewable Energy Research and Development, Guangzhou 510640, China)

**Abstract:** The naturally lackadaisical kinetics of oxygen reduction reaction (ORR) in the cathode is one of the important factors that restrict the development of air-cathode microbial fuel cells (MFCs). In this work, the iron-nitrogen-carbon hierarchically nanostructured materials had been successfully fabricated by pyrolyzing glucose, iron chloride, and dicyandiamide with the aim of solving the issue. The obtained catalyst with an ultrathin nanostructure demonstrated an idiosyncratic electrocatalytic activity caused by the high content introduction of nitrogen and iron atoms, large surface area, which will offer sufficient active sites for improving the charge/mass transfer and reducing the diffusion resistance. Furthermore, with the increase of N dopant in the catalyst, better ORR catalytic activity could be achieved. Illustrating the N doping was beneficial to the ORR process. The high content of N, BET surface area caused by the N increasing could be responsible for the superior performance according to results of X-Ray photoelectron spectroscopy (XPS), Raman and Brunner-Emmet-Teller (BET) analysis. The ORR on the Fe–N<sub>3</sub>/C material follows 4e<sup>-</sup> pathway, and MFCs equipped with Fe–N<sub>3</sub>/C catalyst achieved a maximum power density (MPD) of 912 mW/m<sup>2</sup>, which was 1.1 times of the MPD generated by the commercial Pt/C (830 mW/m<sup>2</sup>). This research not only provided a feasible way for the fabrication of Pt-free catalyst towards oxygen reduction but also proposed potential cathode catalysts for the development of MFCs.

**Keywords:** one-pot pyrolysis route, Fe–N-Doped carbon nanosheets, microbial fuel cells, iron-nitrogen co-doping, carbon based catalyst, electrochemical performance, cathode materials

**DOI:** 10.25165/j.ijabe.20201306.5765

**Citation:** Sun Y, Zhang Z Z, Sun Y M, Yang G X. One-pot pyrolysis route to Fe–N-Doped carbon nanosheets with outstanding electrochemical performance as cathode materials for microbial fuel cell. *Int J Agric & Biol Eng*, 2020; 13(6): 207–214.

## 1 Introduction

Recently, clean energy production, conversion, and storage have been the research focus owing to the scarcity of fossil fuels and their associated environmental problem<sup>[1-6]</sup>. As a promising technology, microbial fuel cells (MFCs) exhibited excellent performance in both electricity production and wastewater treatment<sup>[7-10]</sup>. In MFCs systems, exoelectrogenic microbes degrade the substrate in the anode and release electrons. The protons combined with electrons and electron acceptors (O<sub>2</sub>) at the cathode, and thus generate water eventually. Up to now, the low power and high electrode cost are the main problems that to be solved for the development of MFC. Thus, the commonly used Pt/C catalyst accounting for almost half the cost of an MFCs was hindered by its high cost, rare reservation<sup>[11,12]</sup>, poison caused by the biofilm and pollution due to anions in the media<sup>[13]</sup>. Therefore, the development of an alternative Pt catalyst is significant for the

large-scale application of MFCs.

The application of Pt-free catalysts offers a practicable alternative pathway for reducing the electrode costs and simultaneously enhancing the ORR performance. Among the variety of Pt-free catalysts, nonprecious metal catalysts<sup>[14,15]</sup> and metal-free catalysts<sup>[16]</sup> have been the focus of research owing to their low price, high electrocatalytic performance towards ORR, and long-term stability<sup>[17]</sup>, especially the carbon material with the high quality produced from renewable source<sup>[18]</sup>.

Carbon-based catalysts are promising Pt substitutes for ORR in MFC cathodes, and the desirable four-electron pathway can be achieved along with high current densities and positive onset potentials<sup>[19]</sup>. Additionally, their good anti-biofilm growth ability enhances their feasibility in MFCs by facilitating the use of MFCs in the presence of contaminants and biofilms<sup>[20-22]</sup>.

The ORR property of carbon-based materials will be tuned via the introduction of heteroatom and nonprecious metals, such as nitrogen (N) and iron (Fe)<sup>[23-25]</sup> and cobalt (Co)<sup>[26]</sup>. Notably, even trace amounts of iron in carbon based materials can lead to high electrocatalytic performance and long-term durability<sup>[27-29]</sup> on account of the combined effect between the doped Fe and N, which has been proved to be vital in the ORR process<sup>[30]</sup>. In addition, the nitrogen atoms, especially the pyridinic N, pyrrolic N and graphitic N, affect the ORR activity by changing the electronegativity of the carbonaceous framework and promoting the formation of defects. Besides, the surface area and pore structure of the carbon material also play important roles in

**Received date:** 2020-03-07 **Accepted date:** 2020-11-05

**Biographies:** Zezhen Zhang, Master, research interest: ORR catalyst of MFC, Email: zhangzezhen63@gmail.com; Gaixiu Yang, PhD, Associate Professor, research interest: ORR catalyst of MFC, Email: yanggx@ms.giec.ac.cn.

\*Corresponding author: Yong Sun, PhD, Prof., research interest: anaerobic fermentation. College of Engineering, Northeast Agricultural University, Harbin 150030, China. Tel: +86-13836145034, Email: sunyong740731@163.com; Yongming Sun, PhD, Prof., research interest: anaerobic fermentation. Guangzhou Institute of Energy Conversion, CAS, Guangzhou 510640, China. Tel: +86-13288699886, Email: sunym@ms.giec.ac.cn.

promoting its ORR performance. Many studies confirm the promotion of carbon defects for ORR activity<sup>[31]</sup>. Therefore, fabrication of N and Fe doped carbon-based materials with high specific surface area is of great importance for the development of MFCs.

Numerous literatures have demonstrated that the maximum power density (MPD) generated by using Fe-N/C materials in MFCs cathodes was significantly higher than the MFCs equipped with commercial Pt/C under identical conditions. The MFC equipped with Fe, N decorated carbon material prepared by pyrolyzing the mixture of aniline, Fe(NO<sub>3</sub>)<sub>3</sub>·9H<sub>2</sub>O, ammonium persulfate and anhydrous lithium chloride showed the MPD of 900 mW/m<sup>2</sup>, which is almost twice what the MFC equipped with Pt/C (550 mW/m<sup>2</sup>)<sup>[32]</sup>. Ma et al.<sup>[33]</sup> constructed a Fe-N-C catalyst from living Fe mineral@bacteria encrustation with prominent ORR catalytic property. This performance was similar to the Pt/C catalyst in a neutral electrolyte. Moreover, Fe-ricobenzazole cathode catalysts were fabricated by using ricobenzazole as a carbon and nitrogen source; these catalysts showed better performance than commercial Pt/C when used in MFC cathodes<sup>[19]</sup>. Considering the great potential application of Fe-N co-doped materials in MFCs, it is significant to prepare a Fe-N-C material with plentiful active sites.

Thus, a Fe, N codoped carbon nanosheets with excellent performance towards ORR was fabricated through one-pot pyrolysis. The surface morphology, structure, and chemical composition of the obtained products were systematically studied. Additionally, the effect of N content together with the surface area on the Fe-N/C catalyst with respect to the ORR was also discussed. Further, the performance was demonstrated by these catalysts as cathode materials in MFCs. And the results illustrate that the synthesized catalyst is a promising MFC cathode catalyst.

## 2 Materials and methods

### 2.1 Synthesis of catalysts

The Fe-N<sub>x</sub>/C catalysts were directly synthesized via annealing a mixture of glucose, dicyandiamide (DICY), and FeCl<sub>3</sub>·6H<sub>2</sub>O at 900 °C (Figure 1). Glucose (1 g) and DICY (10 g) were added into 10 mL deionized water (DI water) and subsequently added with 8.0 mL 0.0125 mol/L FeCl<sub>3</sub>·6H<sub>2</sub>O solution. Then it was continuously agitated for 8 h at (25±2) °C. Next, the precursors were placed into a drying oven (60 °C) overnight and then annealed at 900 °C for 2 h. The whole pyrolysis process was protected by continuously N<sub>2</sub>. The final samples were immersed in 1.0 mol/L hydrochloric acid, agitated for 24 h, and then washed by DI water until the pH value of the solution becomes neutral. The obtained products were marked as Fe-N<sub>1</sub>/C.

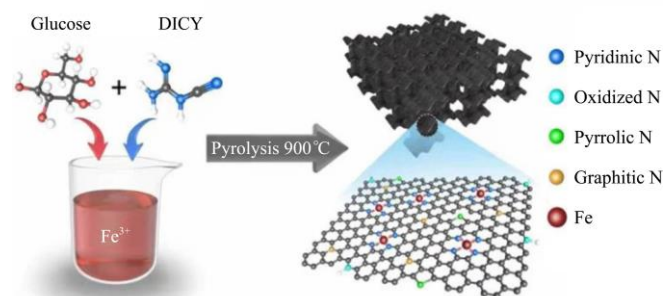


Figure 1 Schematic illustration of the preparation process of Fe-N<sub>x</sub>/C

Similarly, the Fe-N<sub>2</sub>/C and Fe-N<sub>3</sub>/C catalysts were synthesized under the same condition except for the difference in the mass of

DICY, where, the addition of DICY was 20 g for the Fe-N<sub>2</sub>/C catalyst, and 30 g for the Fe-N<sub>3</sub>/C catalyst, respectively.

### 2.2 Aircathode MFC construction and operation

A single chamber air cathode-MFC reactor was constructed, which has a volume of 28 cm<sup>3</sup> with a diameter of 3 cm and a length of 4 cm. The anode of air cathode-MFCs was a carbon fiber brush (CFB), which was annealed at 350 °C for 35 min before use. A carbon cloth with a gas diffusion layer and catalyst layer served as the cathode, its projected area is 7 cm<sup>2</sup>. Carbon black, DI water, and PTFE were mixed and then painted onto the carbon cloth as a gas diffusion layer, as was described in Reference [34]. The prepared Fe-N/C materials were added into a mixture of ethanol, Nafion, and DI water with a volume ratio of 6:1:3, subsequently ultrasonicated for 0.5 h. And then, the ink was painted onto the opposite side of the gas diffusion layer serving as the catalyst layer. The air cathode-MFC equipped with commercial Pt/C (20 wt. %) cathode served as a control sample. The anode microorganism was inoculated from a stable running MFC in the laboratory, then it was fed with phosphate-buffer saline (PBS, 50 mmol/L), sodium acetate (1 g/L), vitamin (5 mL/L), and microelement (12.5 mL/L), as illustrated in Reference [35]. The air cathode MFCs run continuously at (29±0.5) °C in an electro-heating standing-temperature cultivator, which is beneficial for the growth of microorganisms. In addition, the external resistance was 1000 Ω during the period of MFC running. The power density and polarization curves were measured using a steady discharging method by changing the external resistance (99999-80 Ω).

### 2.3 Material characterization and analysis

The X-ray powder diffraction (XRD) patterns were obtained on an X'Pert Pro MPD X-ray diffractometer (Cu Kα X-ray source). The Raman spectra were achieved on a Lab RAM HR800 Raman spectrometer with an excitation wavelength of 785 nm. The X-ray photoelectron spectroscopy (XPS) was obtained on an ESCALAB 250Xi spectrometer. XPS-peak was used to fit the XPS data of each element. N<sub>2</sub> sorption isotherms were measured on an IQ-2 analyzer at 77 K. Scanning electron microscopy (SEM, Hitachi s-4800) and transmission electron microscopy (TEM, Hitachi JEM-2100) were used to investigate the morphologies of obtained materials.

### 2.4 Electrochemical measurement

Electrochemical experiments were conducted on the CHI660E electrochemical workstation. The working electrode is a glassy carbon electrode (5 mm diameter, 0.19625 cm<sup>2</sup> geometric area) modified with catalyst, saturated calomel electrode (SCE) was used as the reference electrode, and Pt wire served as the counter electrodes. The catalyst mixture was obtained by adding 9.8 mg of as-prepared catalyst into the mixture of Nafion, ethanol and DI-water with a volume of 1 mL at a volume ratio of 3:5:2, then ultrasonicated for 20 min. Rotating disk electrode (RDE) tests were conducted from the potential of -0.6 V to 0.6 V in a nitrogen/oxygen-saturated 50 mmol/L PBS solution at various rotation speeds (400 r/min, 900 r/min, 1600 r/min and 2500 r/min) with a scan rate of 50 mV/s. All the electrochemical experiments were repeated three times, the average values of three tests were used. The electron transferred number (*n*) was obtained by Koutecky-Levich (K-L) Equation (1).

$$\frac{1}{J} = \frac{1}{J_K} + \frac{1}{0.2nFC_0D_0^{2/3}v^{-1/6}\omega^{1/2}} \quad (1)$$

where, *J* and *J<sub>K</sub>* are the measured and kinetic current density, mA/cm<sup>2</sup>, respectively; *ω* represents the rotating speed, r/min; *F* is

the Faraday constant;  $C_0$  is the bulk concentration of oxygen ( $C_0=1.1\times 10^{-6}$  mol/L),  $D_0$  is the  $O_2$  diffusion coefficient ( $D_0=1.4\times 10^{-5}$  mol  $cm^2/s$ );  $\nu$  is the kinematic viscosity of the electrolyte ( $\nu=0.01$   $cm^2/s$ ).

### 3 Results and discussion

#### 3.1 Characterization of catalyst structure and morphology

The morphology and microstructural features of the Fe-N<sub>1</sub>/C, Fe-N<sub>2</sub>/C and Fe-N<sub>3</sub>/C catalysts which were prepared by pyrolyzing the mixture of dicyandiamide, FeCl<sub>3</sub>·6H<sub>2</sub>O and glucose at 900 °C under an N<sub>2</sub> atmosphere were analyzed by SEM, TEM, and element mapping. Low-resolution SEM images (Figures 2a-2c) show corrugated carbon sheets. Fe-N<sub>3</sub>/C (which had the highest DICY content among the three catalysts) possesses a more ultra-thin and hieratical structure than the stacked morphology and thick carbon

nanosheets of Fe-N<sub>1</sub>/C and Fe-N<sub>2</sub>/C as shown in Figure 3. The TEM was conducted to investigate the microstructure of the products. Figures 2d-2f show the typical microstructure features of graphene nanosheets with abundant wrinkles present on their surface. As reported by Boukhvalov et al.<sup>[36]</sup> O<sub>2</sub> adsorption on the catalyst surface can be enhanced by the abundant microstructures and high surface area, which is beneficial for the ORR process. Elemental mapping was performed to analyze the elemental distributions in the obtained catalysts; N and Fe were uniformly dispersed throughout the graphene nanosheets in all selected regions (Figures 2g-2i). Thus, the synthetic route produced the Fe-N<sub>x</sub>/C catalysts with N and Fe atoms homogeneously embedded into the carbon matrix. The N content was easily tunable by adding an appropriate amount of nitrogen precursor in the reaction system.

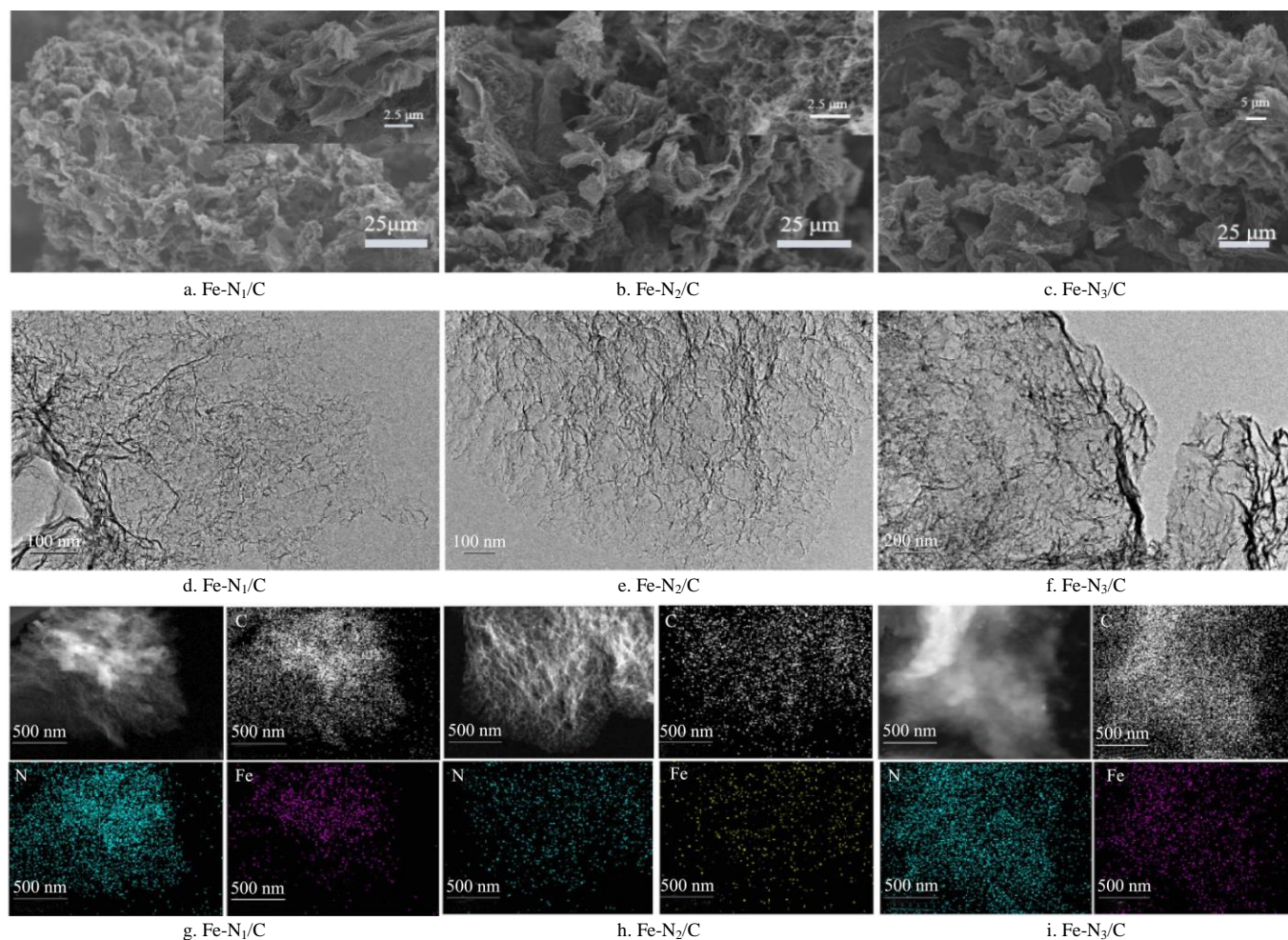


Figure 2 SEM images of (a) Fe-N<sub>1</sub>/C, (b) Fe-N<sub>2</sub>/C and (c) Fe-N<sub>3</sub>/C, TEM images of (d) Fe-N<sub>1</sub>/C, (e) Fe-N<sub>2</sub>/C and (f) Fe-N<sub>3</sub>/C. Corresponding elemental mapping of atomically dispersed of (g) Fe-N<sub>1</sub>/C, (h) Fe-N<sub>2</sub>/C and (i) Fe-N<sub>3</sub>/C

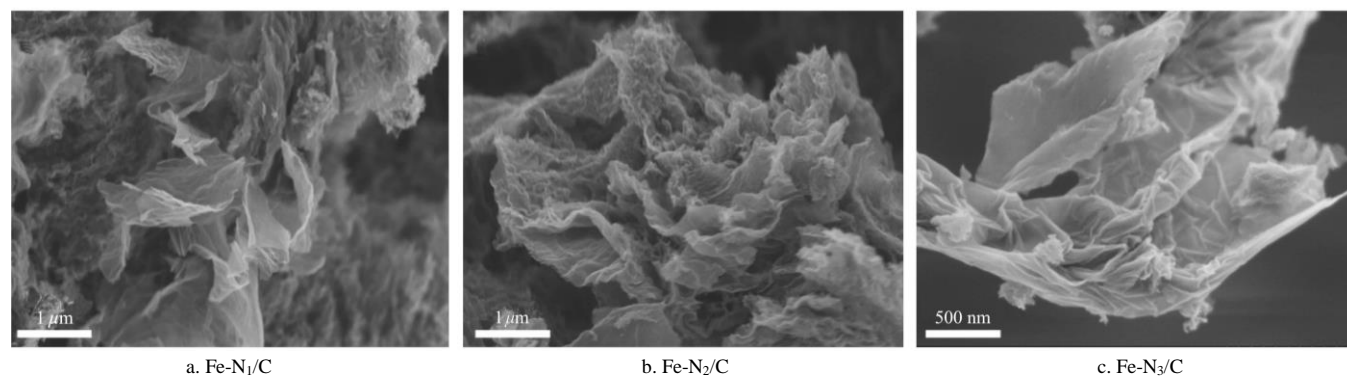


Figure 3 SEM images of Fe-N<sub>1</sub>/C, Fe-N<sub>2</sub>/C and Fe-N<sub>3</sub>/C

The structures of the prepared catalysts were examined by XRD. From the XRD patterns of as-prepared catalysts (Figure 4a), it can be seen that the peaks appeared at the neighborhood of  $26.5^\circ$  and  $43.7^\circ$  for the three catalysts corresponded to the (002) and (101) lattice planes of graphite, respectively<sup>[37]</sup>. The (002) diffraction peak was caused by the graphitic structure, indicating an interlayer spacing of 0.34 nm. On the other hand, the (101) diffraction peak was induced by the fibrous/spherical structures formed by  $sp^2$  hybridized carbons in the sample, owing to the low degree of graphitization<sup>[38]</sup>. The intensity of (101) diffraction peak decreased with the increasing N content, implying that N doping and rearrangement of the graphitic structure occurred in the synthetic procedure, generated a large number of defects, and promoted the ORR activity; similar results have been reported by Xia et al.<sup>[39]</sup> No Fe or  $Fe_xO_y$  diffraction peaks were observed for any of the synthesized catalysts, indicating that the Fe atoms

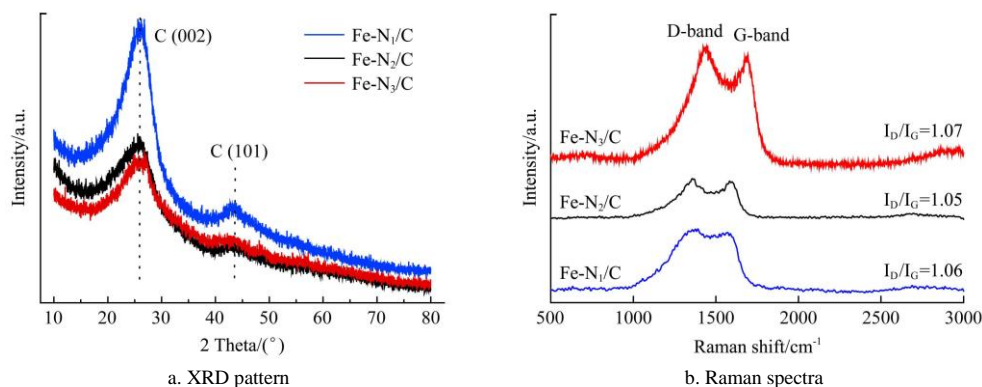


Figure 4 (a) XRD pattern, (b) Raman spectra of Fe-N<sub>1</sub>/C, Fe-N<sub>2</sub>/C and Fe-N<sub>3</sub>/C

The XPS analysis was carried out to determine the surface component and composition of obtained Fe-N/C materials. The XPS spectrum confirms the existence of C, N, O, and traces of Fe in Fe-N/C (Figure 5a). The N1s XPS peaks for the as-prepared products were further decomposed into the peaks of four N-containing functional groups: pyridinic N (398.1 eV), pyrrolic N (400.5 eV), graphitic N (401.9 eV), and oxidized N (405.0 eV)<sup>[42]</sup>, as displayed in Figures 5b-5d. The XPS survey data for Fe-N<sub>1</sub>/C, Fe-N<sub>2</sub>/C, and Fe-N<sub>3</sub>/C and the percentages of various nitrogen species are shown in Table 1. Compared with the other two samples, Fe-N<sub>3</sub>/C possesses the higher pyridinic N (4.89 at. %) and pyrrolic N (5.46 at. %) content compared with the other two catalysts, and the pyridinic N has been proved by Guo et al.<sup>[43]</sup> that it generates active sites via utilizing newly fabricated graphite model materials. Relevant research also proved that O<sub>2</sub> adsorption energy could be reduced by the introduction of pyridinic N and pyrrolic N<sup>[44]</sup>, in addition, the large amount of pyridinic N facilitates the ORR process via a  $4e^-$  pathway<sup>[45]</sup>.

**Table 1** XPS parameters from N1s peak fitting of Fe-N<sub>1</sub>/C, Fe-N<sub>2</sub>/C and Fe-N<sub>3</sub>/C (at. %)

	N content	Pyridinic-N	Pyrrolic-N	Graphitic-N	Oxidized N
Fe-N <sub>1</sub> /C	8.30	4.36	2.92	0.62	0.40
Fe-N <sub>2</sub> /C	10.85	4.69	5.03	0.90	0.21
Fe-N <sub>3</sub> /C	10.96	4.89	5.46	0.45	0.15

The high-resolution Fe2p XPS spectra (Figures 5f and 5g) of Fe-N<sub>2</sub>/C and Fe-N<sub>3</sub>/C were decomposed into two asymmetric well-resolved doublets, which are corresponding to Fe2p<sub>3/2</sub> and Fe2p<sub>1/2</sub>. The Fe2p<sub>3/2</sub> and Fe2p<sub>1/2</sub> peaks could be further divided into two peaks. The peaks located at 713.0 eV and 723.8 eV corresponded to Fe(II)2p<sub>3/2</sub> and Fe(II)2p<sub>1/2</sub>, while the peaks located

existed in the carbon matrix in a disordered form or the amount of Fe was too low to be examined by XRD<sup>[40]</sup>. Figure 4b displays the Raman spectra of the Fe-N<sub>1</sub>/C, Fe-N<sub>2</sub>/C, and Fe-N<sub>3</sub>/C catalysts. G-band originating from the in-plane stretching vibrations of all  $sp^2$  hybrid atoms, such as C=C and C-N, in the graphitic structure are located at  $\sim 1340\text{ cm}^{-1}$ . D-band relating to the defects and disordered structures that are caused by vacancies and heteroatom doping are located at  $1583\text{ cm}^{-1}$ <sup>[41]</sup>. The value of  $I_D/I_G$  is served as an indicator to investigate the defects and graphitic degree of the catalysts. Notably, the  $I_D/I_G$  ratio for Fe-N<sub>3</sub>/C (1.07) was larger than those for Fe-N<sub>1</sub>/C (1.06) and Fe-N<sub>2</sub>/C (1.05); this could be attributed to the introduction of a large number of N into the carbonaceous framework, which could generate numerous active sites in the obtained catalysts<sup>[19,30]</sup>. It is conducive for oxygen chemisorption, and they subsequently promote the rate of the ORR process.

at 710.8 eV and 726.1 eV corresponded to Fe(III)2p<sub>3/2</sub> and Fe(III)2p<sub>1/2</sub><sup>[46]</sup>. This demonstrates that the Fe species has been successfully introduced.

N<sub>2</sub> adsorption-desorption tests were executed for Fe-N<sub>x</sub>/C to measure their Brunner-Emmet-Teller (BET) surface areas and pore size distribution (PSD). As shown in Figure 6, all samples exhibited type III isotherms. The pore size distribution (Figure 6b) also further proved that the Fe-N<sub>x</sub>/C materials mainly consist of mesoporous and microporous structures. The BET surface area of Fe-N<sub>3</sub>/C was 1146 m<sup>2</sup>/g, which is larger than the other two; the surface areas of Fe-N<sub>1</sub>/C and Fe-N<sub>2</sub>/C were 221 m<sup>2</sup>/g and 453 m<sup>2</sup>/g, respectively. This demonstrates that nitrogen content in the catalyst could increase the BET surface area. Generally, a large BET surface is beneficial for the formation of active centers on the catalyst surface, and abundant pore channels can improve the efficiency of oxygen transportation.

### 3.2 Electrochemically catalytic activity

Linear sweep voltammetry (LSV) was used to evaluate the ORR performance of the obtained catalysts in 50 mmol/L PBS saturated with O<sub>2</sub> at 50 mV/s (Figure 7a). The onset potentials for the prepared catalysts and the commercial Pt/C for ORR are in the order of Fe-N<sub>3</sub>/C, Pt/C, Fe-N<sub>2</sub>/C, Fe-N<sub>1</sub>/C, indicating the distinguished ORR catalytic ability of the Fe-N<sub>3</sub>/C material. Evidently, the Fe-N<sub>3</sub>/C demonstrated a significant positive shift in the half-wave potential ( $-63\text{ mV}$ ) relative to that of the Pt/C catalyst ( $-77\text{ mV}$ ). Moreover, positive shifts of 35 mV and 50 mV can be found for the Fe-N<sub>3</sub>/C catalyst, compared with those for the Fe-N<sub>2</sub>/C ( $-98\text{ mV}$ ) and Fe-N<sub>1</sub>/C ( $-113\text{ mV}$ ) catalysts. This suggested that by increasing the DICY amount in the reaction system, the electrocatalytic performance of Fe-N<sub>x</sub>/C catalysts could be enhanced. This enhancement could be ascribed to 1) increase

in the introduction of N functional groups, particularly pyridinic N and pyrrolic N, which have been proved to be vital in the ORR process; 2) large BET surface area which offers plentiful active centers during the ORR process. Furthermore, the ORR kinetics in neutral media were evaluated by the Koutecky-Levich equation. As depicted in Figure 7c, the LSV curves for Fe-N<sub>3</sub>/C were obtained from RDE under various electrode rotating speeds (400-2500 r/min) in the O<sub>2</sub>-saturated neutral electrolyte. The electron transfer number for Fe-N<sub>3</sub>/C is 4.05 at -0.45 V (vs SCE). This result suggests that the ORR followed an ideal four-electron

path on the Fe-N<sub>3</sub>/C catalyst. The specific kinetic current density ( $i_k$ ) is a typical indicator of the intrinsic catalytic activity for a catalyst. The plots of E vs.  $\log i_k$  are exhibited in Figure 7b the  $i_k$  value for Fe-N<sub>3</sub>/C catalyst was greater than that for the commercial Pt/C under the same potential, thereby demonstrating predominant catalytic activity of the Fe-N<sub>3</sub>/C catalyst. A large BET surface area and meso/macropore hierarchical pore size distribution together with the high N content of the Fe-N<sub>3</sub>/C catalyst could be responsible for its excellent electrocatalytic performance.

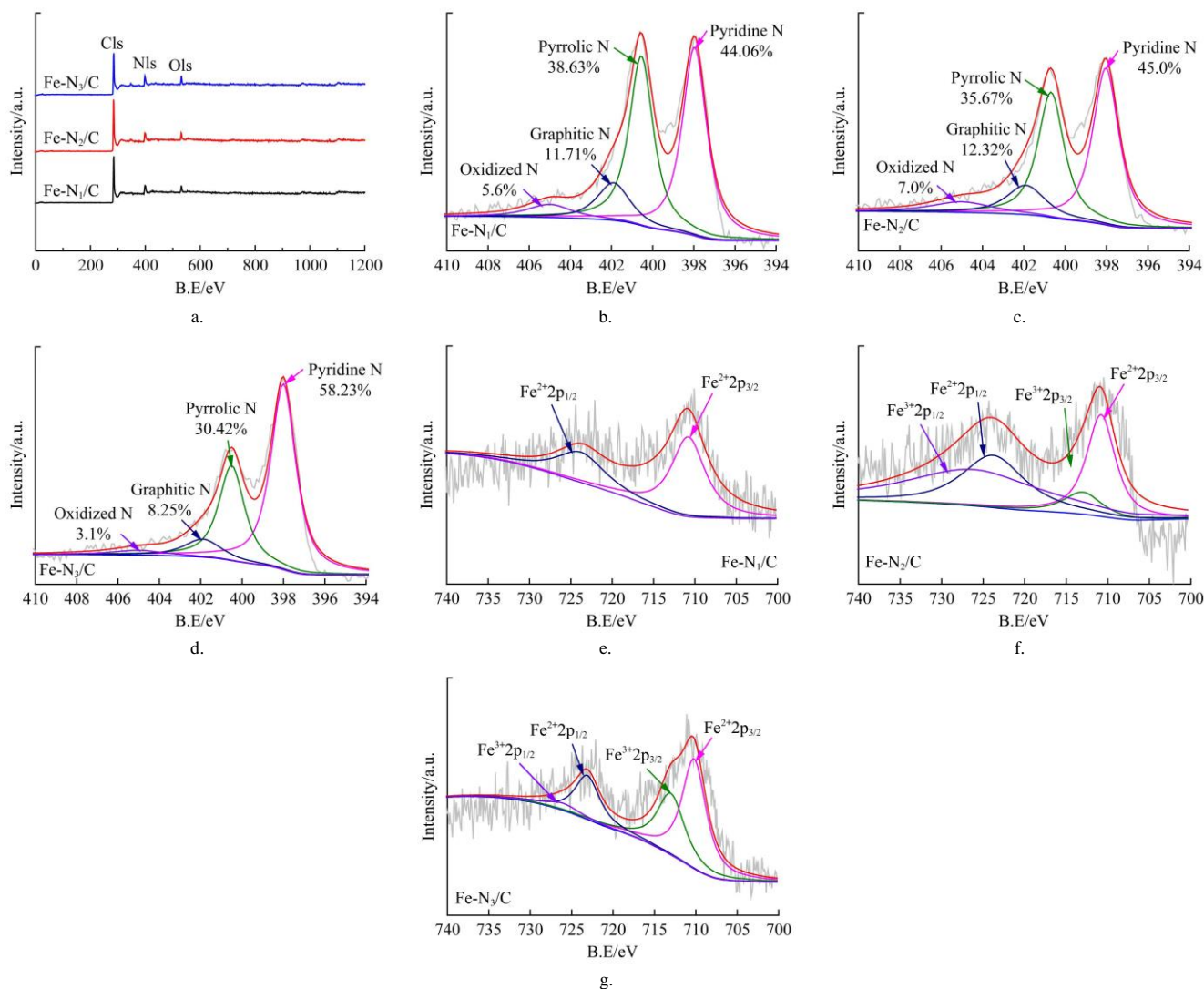


Figure 5 (a) XPS spectra of Fe-N<sub>1</sub>/C, Fe-N<sub>2</sub>/C and Fe-N<sub>3</sub>/C, (b-d) High-resolution N1s, (e-f) High-resolution Fe2p of Fe-N<sub>2</sub>/C, Fe-N<sub>3</sub>/C

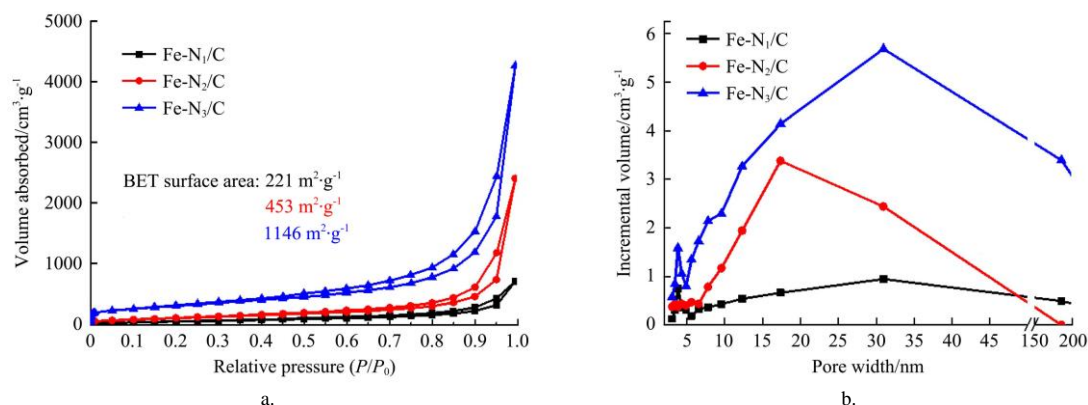


Figure 6 (a) N<sub>2</sub> sorption isotherms of Fe-N<sub>1</sub>/C, Fe-N<sub>2</sub>/C and Fe-N<sub>3</sub>/C. (b) Pore-size distributions (PSDs) of the Fe-N<sub>1</sub>/C, Fe-N<sub>2</sub>/C and Fe-N<sub>3</sub>/C

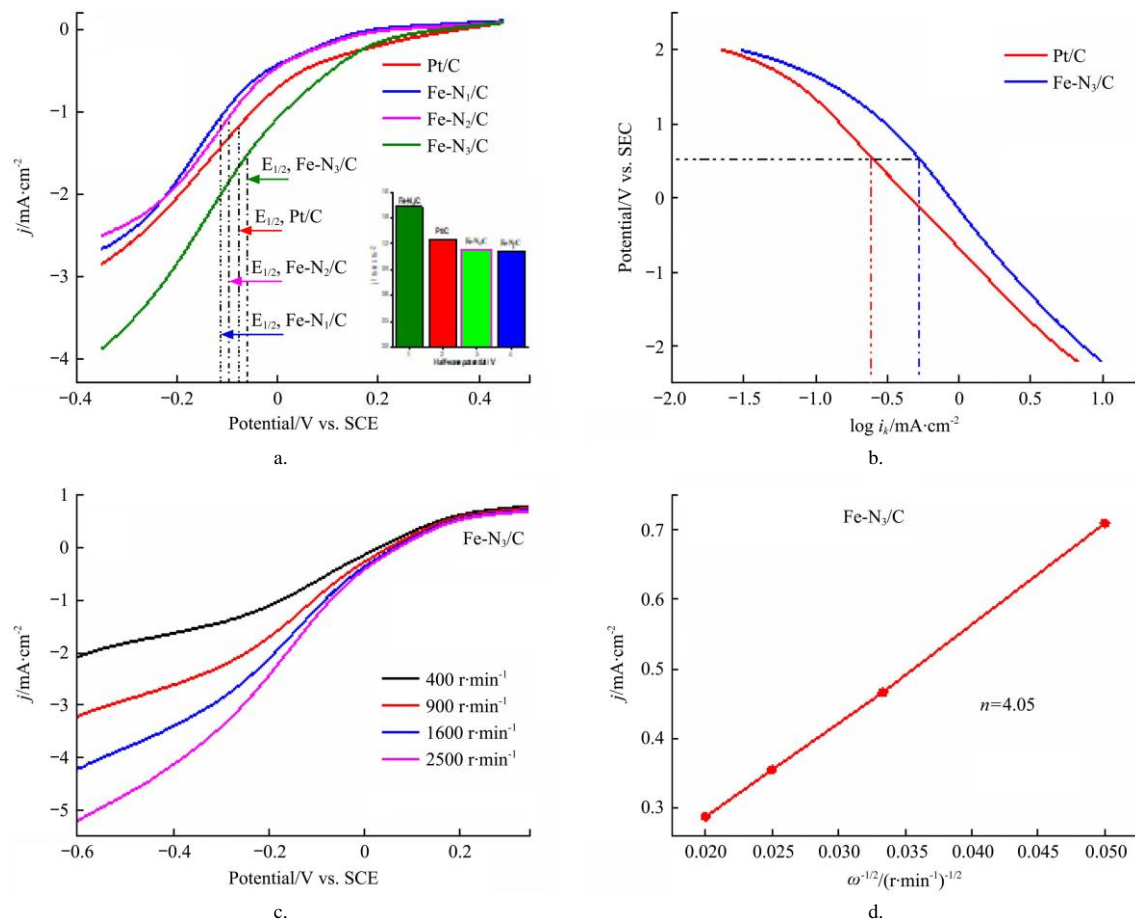


Figure 7 (a) LSV curves of Fe-N<sub>1</sub>/C, Fe-N<sub>2</sub>/C and Fe-N<sub>3</sub>/C and the commercial Pt/C with the scan rate of 50 mV/s in O<sub>2</sub> saturated 50 mM PBS electrolytes (1600 r/min); (b) Tafel plots of Fe-N<sub>3</sub>/C and the commercial Pt/C; (c) LSV curves of Fe-N<sub>3</sub>/C with various rotation rates at a scan rate of 50 mV/s; (d) Koutecky-Levich plot of Fe-N<sub>3</sub>/C in -0.45 V (vs. SCE)

To demonstrate the property of the prepared catalysts in MFCs, Fe-N<sub>3</sub>/C catalyst whose loading is 0.5 mg/cm<sup>2</sup>, was employed in an MFC cathode, while the commercial Pt/C catalyst served as a contrast with respect to voltage output and power output. According to Figure 8, the MPD of the air-cathode MFCs with Fe-N<sub>3</sub>/C catalyst as the cathodic ORR catalyst is 912 mW/m<sup>2</sup>, while the MPD is generated by the MFCs assembled with Pt/C catalyst is 834 mW/m<sup>2</sup>. In contrast to the Pt/C catalyst, the MFCs with Fe-N<sub>3</sub>/C catalyst exhibited a higher MPD, indicating that

Fe-N-C shows priority property in the practical operation of MFCs. The high content of N; hierarchical pore size distribution; and larger BET surface area could mainly account for the excellent ORR performance of the MFC assembled with the Fe-N<sub>3</sub>/C catalyst, compared with that using the Pt/C catalyst. A mass of active centers could be offered through the Fe-N<sub>3</sub>/C catalyst for accepting the electrons transferred from the anode. Moreover, the unique structure of the Fe-N<sub>3</sub>/C material can accelerate the oxygen diffusion, adsorption, and dissociation process.

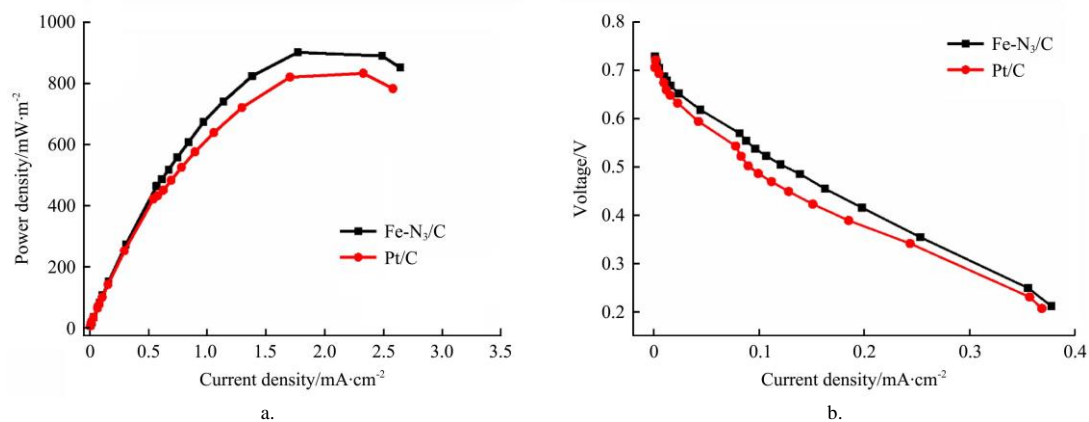


Figure 8 (a) Power density (PD) and (b) polarization curves of MFCs assembled with Fe-N<sub>3</sub>/C and Pt/C cathodes fed with 1 g/L sodium acetate in neutral phosphate buffer (PBS)

## 4 Conclusions

In summary, the Fe-N<sub>x</sub>/C materials with different contents of added DICY (added into the reaction system) were successfully

synthesized, and the influence of N content on the ORR performance was further investigated about onset potential and half-wave potential. The higher power density and voltage output of Fe-N<sub>3</sub>/C catalyst are due to the abundance of active sites, large

BET surface area, and hierarchical pore size distribution. The porous structure is conducive to accelerating the oxygen mass transfer, and the introduction of N in the carbonaceous framework offers numerous active sites for the decomposition of O<sub>2</sub> by weakening the O-O bond. Additionally, the ORR catalytic performance was enhanced with the increasing amount of N precursor. The Fe-N<sub>3</sub>/C catalyst exhibited an MPD of 912 mW/m<sup>2</sup>, which was 1.1 times that of Pt/C catalyst (830 mW/m<sup>2</sup>). The higher activity indicated that the Fe-N<sub>3</sub>/C catalyst is a potential alternative for Pt/C in MFCs for ORR.

## Acknowledgements

This work was financially supported by the National Natural Science Foundation of China (Grant No. 51806224); Natural Science Foundation of Guangdong Province (Grant No. 2017A030310280); the Strategic Priority Research Program of the Chinese Academy of Sciences (Grant No. XDA21050400); the China Postdoctoral Science Foundation (Grant No. 2018M631899). The authors acknowledge the care and spiritual support from Gaixiu Yang over the past two years.

## [References]

- Chen P, Wang L K, Wang G, Gao M R, Ge J, Yuan W J, et al. Nitrogen-doped nanoporous carbon nanosheets derived from plant biomass: An efficient catalyst for oxygen reduction reaction. *Energy Environ. Sci.*, 2014; 7: 4095–4103.
- Seh Z W, Kibsgaard J, Dickens C F, Chorkendorff I B, Norskov J K, Jaramillo T F. Combining theory and experiment in electrocatalysis: Insights into materials design. *Science*, 2017; 355: 1. doi: 10.1126/science.aad4998.
- Zhao Y S, Wan J W, Yao H Y, Zhang L J, Lin K F, Wang L, et al. Few-layer graphdiyne doped with sp-hybridized nitrogen atoms at acetylenic sites for oxygen reduction electrocatalysis. *Nat. Chem.*, 2018; 10: 924–931.
- Liu J, Jiao M G, Lu L L, Barkholtz H M, Li Y P, Wang Y, et al. High performance platinum single atom electrocatalyst for oxygen reduction reaction. *Nat. Commun.*, 2017; 8: 1. doi: 10.1038/ncomms16160.
- Liu C Y, Sun Y, Li N, Zhang B, Liu J M. Improved energy utilization efficiency via adding solar radiant heating mode for traditional bioreactor to dispose straw: Experimental and numerical evaluation. *Waste Management*, 2019; 89: 303–312.
- Wang Z, Cheng Q S, Qu J B, Chu X D, Li N, Noor R S, et al. Evaluation of methane production and energy conversion from corn stalk using furfural wastewater pretreatment for whole slurry anaerobic co-digestion. *Bioresour. Technol.*, 2019; 293: 121962. doi: 10.1016/j.biortech.2019.121962.
- Li W W, Yu H Q, He Z. Towards sustainable wastewater treatment by using microbial fuel cells-centered technologies. *Energy Environ. Sci.*, 2014; 7: 911–924.
- Wu H J, Guo C Z, Li J Q, Ma Z L, Feng Q Y, Chen C G. A graphene-based electrocatalyst co-doped with nitrogen and cobalt for oxygen reduction reaction. *Int. J. Hydrog. Energy*, 2016; 41(45): 20494–20501.
- Yang Z R, Wu J, Zheng X J, Wang Z J, Yang R Z. Enhanced catalytic activity for the oxygen reduction reaction with co-doping of phosphorus and iron in carbon. *J. Power Sources* 2015; 277: 161–168.
- Bi L L, Ci S Q, Cai P W, Li H, Wen Z H. One-step pyrolysis route to three dimensional nitrogen-doped porous carbon as anode materials for microbial fuel cells. *Appl. Surf. Sci.*, 2018; 427: 10–16.
- Bai L, Duan Z Y, Wen X D, Si R, Guan J Q. Atomically dispersed manganese-based catalysts for efficient catalysis of oxygen reduction reaction. *Appl. Catal. B-Environ.*, 2019; 257: 7. doi: 10.1016/j.apcatb.2019.117930.
- Wang S Y, Zhang L P, Xia Z H, Roy A, Chang D W, Baek J B, et al. BCN Graphene as Efficient Metal-Free Electrocatalyst for the Oxygen Reduction Reaction. *Angew. Chem.-Int. Edit.*, 2012; 51: 4209–4212.
- Xia W, Mahmood A, Liang Z B, Zou R Q, Guo S J. Earth-Abundant Nanomaterials for Oxygen Reduction. *Angew. Chem.-Int. Edit.*, 2016; 55: 2650–2676.
- Jing B J, Ma Y Y, Xing Z, Chen H, Dai Y, Zhang C Y, et al. Fe<sub>3</sub>Se<sub>4</sub>/FeSe heterojunctions in cornstalk-derived N-doped carbon framework enhance charge transfer and cathodic oxygen reduction reaction to boost bio-electricity generation. *Appl. Catal. B-Environ.*, 2019; 244: 465–474.
- Guo D K, Tian Z F, Wang J C, Ke X B, Zhu Y F. Co<sub>2</sub>N nanoparticles embedded N-doped mesoporous carbon as efficient electrocatalysts for oxygen reduction reaction. *B Appl. Surf. Sci.*, 2019; 473: 555–563.
- Majidi M R, Farahani F S, Hosseini M, Ahadzadeh I. Low-cost nanowired alpha-MnO<sub>2</sub>/C as an ORR catalyst in air-cathode microbial fuel cell. *Bioelectrochemistry*, 2019; 125: 38–45.
- Cai T, Huang Y X, Huang M H, Xi Y, Pang D Y, Zhang W. Enhancing oxygen reduction reaction of supercapacitor microbial fuel cells with electrospun carbon nanofibers composite cathode. *Chem. Eng. J.*, 2019; 371: 544–553.
- Marsudi M A, Ma Y, Prakoso B, Hutani J J, Wibowo A, Zong Y, et al. Manganese oxide nanorods decorated table sugar derived carbon as efficient bifunctional catalyst in rechargeable Zn-air batteries. *Catalysts*, 2020; 10: 64. doi: 10.3390/csts110010064.
- Santoro C, Serov A, Gokhale R, Rojas-Carbonell S, Stariha L, Gordon J, et al. A family of Fe-N-C oxygen reduction electrocatalysts for microbial fuel cell (MFC) application: Relationships between surface chemistry and performances. *Appl. Catal. B-Environ.*, 2017; 205: 24–33.
- Zhang X Y, Pant D, Zhang F, Liu J, He W H, Logan B E. Long-term performance of chemically and physically modified activated carbons in air cathodes of microbial fuel cells. *ChemElectroChem*, 2014; 1: 1859–1866.
- Yellappa M, Sravan J S, Sarkar O, Reddy Y V R, Mohan S V. Modified conductive polyaniline-carbon nanotube composite electrodes for bioelectricity generation and waste remediation. *Bioresour. Technol.*, 2019; 284: 148–154.
- Logan B, Zikmund E, Yang W, Rossin R, Kim K, Saikaly P, et al. Increasing power generation in a continuous flow MFC by advective flow through the porous anode and reduced electrode spacing. *Environ. Sci. Technol.*, 2005; 40(7): 2426–2432.
- Zhang Y J, Lu L H, Zhang S, Lyu Z Z, Yang T, Liu J H, et al. Biomass chitosan derived cobalt/nitrogen doped carbon nanotubes for the electrocatalytic oxygen reduction reaction. *J. Mater. Chem. A.*, 2018; 6: 5740–5745.
- Xie Y, Li H Q, Tang C Z, Li S S, Li J, Lyu Y, et al. A high-performance electrocatalyst for oxygen reduction based on reduced graphene oxide modified with oxide nanoparticles, nitrogen dopants, and possible metal-N-C sites. *J. Mater. Chem. A.*, 2014; 2: 1631–1635.
- Wu G, More K L, Johnston C M, Zelenay P. High-performance electrocatalysts for oxygen reduction derived from polyaniline, iron, and cobalt. *Science*, 2011; 332: 443–444.
- An T, Ge X, Tham N N, Sumbhoj A, Liu Z, Zong Y. Facile one-pot synthesis of coFe alloy nanoparticles decorated N-doped carbon for high-performance rechargeable Zinc-air battery stacks. *ACS Sustainable Chem. Eng.*, 2018; 6: 7743. doi: 10.1021/acssuschemeng.8b00657.
- Masa J, Xia W, Muhler M, Schuhmann W. On the role of metals in nitrogen-doped carbon electrocatalysts for oxygen reduction. *Angew. Chem.-Int. Edit.*, 2015; 54: 10102–10120.
- Li G N, Zheng K T, Xu C J. An ingenious approach for ZIFs derived N-doped hierarchical porous carbon hybrids with FeCo alloy nanoparticles as efficient bifunctional oxygen electrocatalysts. *Appl. Surf. Sci.*, 2019; 487: 496–502.
- Nguyen C V, Lee S, Chung Y G, Chiang W H, Wu K C W. Synergistic effect of metal-organic framework-derived boron and nitrogen heteroatom-doped three-dimensional porous carbons for precious-metal-free catalytic reduction of nitroarenes. *Appl. Catal. B-Environ.*, 2019; 257: 117888. doi: 10.1016/j.apcatb.2019.117888.
- Lin L, Qing Z, Xu A W. Noble metal-free Fe-N/C catalyst for highly efficient oxygen reduction reaction under both alkaline and acidic conditions. *J. Am. Chem. Soc.*, 2015; 249: 1. doi: 10.1021/ja504696r.
- Jiang Y, Yang L, Su T, Zhao J, Lyu Z, Zhuo O, et al. Significant contribution of intrinsic carbon defects to oxygen reduction activity. *ACS Catalysis*, 2015; 5: 6707–6712.
- Ren P Y, Ci S Q, Ding Y C, Wen Z H. Molten-salt-mediated synthesis of porous Fe-containing N-doped carbon as efficient cathode catalysts for microbial fuel cells. *Appl. Surf. Sci.*, 2019; 481: 1206–1212.
- Ma X X, Lei Z C, Feng W M, Ye Y L, Feng C H. Living Fe mineral@bacteria encrustation-derived and self-templated preparation of a

- mesoporous Fe-N-C electrocatalyst with high activity for oxygen reduction. *Carbon*, 2017; 123: 481–491.
- [34] Yuan Y, Zhou S G, Xu N, Zhuang L. Microorganism-immobilized carbon nanoparticle anode for microbial fuel cells based on direct electron transfer. *Appl. Microbiol. Biotechnol.*, 2011; 89: 1629–1635.
- [35] Yang G X, Wang Y F, Xu L B, Li Y, Li L H, Sun Y M, et al. Pd nanochains: Controlled synthesis by lysine and application in microbial fuel cells. *Chem. Eng. J.*, 2020; 379: 8. doi: 10.1016/j.cej.2019.122230.
- [36] Boukhvalov D W, Katsnelson M I. Enhancement of chemical activity in corrugated graphene. *J. Phys. Chem. C*, 2009; 113: 14176–14178.
- [37] Bayram E, Yilmaz, G, Mukerjee S. A solution-based procedure for synthesis of nitrogen doped graphene as an efficient electrocatalyst for oxygen reduction reactions in acidic and alkaline electrolytes. *Appl. Catal. B-Environ.*, 2016; 192: 26–34.
- [38] Wang C H, Yang C W, Lin Y C, Chang S T, Chang S L Y. Cobalt-iron (II, III) oxide hybrid catalysis with enhanced catalytic activities for oxygen reduction in anion exchange membrane fuel cell. *J. Power Sources*, 2015; 277: 147–154.
- [39] Sheng Z H, Shao L, Chen J J, Bao W J, Wang F B, Xia X H. Catalyst-Free synthesis of nitrogen-doped graphene via thermal annealing graphite oxide with melamine and its excellent electrocatalysis. *ACS Nano*, 2011; 5: 4350–4358.
- [40] Wang J, Wang G X, Miao S, Jiang X L, Li J Y, Bao X H. Synthesis of Fe/Fe<sub>3</sub>C nanoparticles encapsulated in nitrogen-doped carbon with single-source molecular precursor for the oxygen reduction reaction. *Carbon*, 2014; 75: 381–389.
- [41] Wang X X, Cullen D A, Pan Y T, Hwang S, Wang M, Feng Z, et al. Nitrogen-coordinated single cobalt atom catalysts for oxygen reduction in proton exchange membrane fuel cells. *Adv. Mater.*, 2018; 30. doi: 10.1002/adma.201706758.
- [42] Sun Y, Duan Y Q, Hao L, Xing Z P, Dai Y, Li R, et al. Cornstalk-derived nitrogen-doped partly graphitized carbon as efficient metal-free catalyst for oxygen reduction reaction in microbial fuel cells. *ACS Appl. Mater. Interfaces*, 2016; 8: 25923–25932.
- [43] Guo D, Shibuya R, Akiba C, Saji S, Kondo T, Nakamura J. Active sites of nitrogen-doped carbon materials for oxygen reduction reaction clarified using model catalysts. *Science*, 2016; 351: 361–365.
- [44] Feng L, Yan Y, Chen Y, Wang L. Nitrogen-doped carbon nanotubes as efficient and durable metal-free cathodic catalysts for oxygen reduction in microbial fuel cells. *Energy Environ. Sci.*, 2011; 4: 1892. doi: 10.1039/c1ee01153g.
- [45] Lai L F, Potts J R, Zhan D, Wang L, Poh C K, Tang C H, et al. Exploration of the active center structure of nitrogen-doped graphene-based catalysts for oxygen reduction reaction. *Energy Environ. Sci.*, 2012; 5: 7936–7942.
- [46] Battez A, Gonzalez R, Viesca J L, Blanco D, Asedegbega E, Osorio A. Tribological behaviour of two imidazolium ionic liquids as lubricant additives for steel/steel contacts. *Wear*, 2009; 266: 1224–1228.